NUMERICAL SIMULATION OF FLOW FIELDS IN LARGE-SCALE SEGMENTED-TYPE ARC HEATERS

Yusuke Takahashi , Hisashi Kihara , Ken-ichi Abe
***Department of Aeronautics and Astronautics, Kyushu University**

Keywords: *Arc-heated flow, radiation, turbulence, numerical simulation*

Abstract

Turbulent plasma flow in large-scale arc heater such as NASA 60 MW Interaction Heating Facility was numerically investigated and the distribution of the arc-heated flow-field properties were successfully obtained. The turbulent flow-field was described by the Reynolds-Averaged Navier-Stokes equations with a multi-temperature model, tightly coupled with the electric field and the radiation-field calculations. In addition, an accurate and low-cost radiation model and a low-Reynolds number two-equation turbulence model were introduced into the flow-field simulation. It was quantitatively clarified that radiation and turbulence phenomena are very important mechanisms to transfer heat and momentum from high-temperature core region to cold gas region near the wall. To validate the present numerical model, the numerical solutions were compared with the experimental data, e.g., arc voltage, mass-averaged enthalpy, chamber pressure and heat efficiency. It was indicated that the present flow-field simulation model showed good agreement over various operating conditions of the facilities.

1 Introduction

An arc-heated wind tunnel is very useful for ground-based experiments of the planet-entry environment. Its applications include the performance test of a thermal protection system (TPS) and the development of an ablator. To perform such an experiment with high quality, it is indispensable to understand the correct physical properties of the free jet discharged from the nozzle exit. In an arc heater, however, the flow field is very complicated due to complex phenomena of the heating process in the constrictor as well as the strong thermochemical nonequilibrium in the nozzle [1]. Therefore, it is extremely difficult to measure all the properties of the free jet simultaneously. On the other hand, with remarkable development of high-performance computers, numerical predictions have now become powerful tools for investigating the details of such complex flow fields.

Several efforts have focused on identifying the arc-heated flow properties such as enthalpy, temperature, velocity and species concentration by use of computational fluid dynamics (CFD) [2–7]. For accurate prediction of the flow-property distributions in an arc-heated flow simulation, it is important to correctly calculate the heating process in the constrictor section and the expansion phenomena in the nozzle section. In order to model the heating-section on the constrictor correctly, it is preferable to calculate the flow field coupled with the electric field calculation. Additionally, accurate treatment of the radiation heat transport is also important. At the same time, since the expansion flow in the nozzle section excites rotationally and vibrationally, and strong thermal nonequilibrium appears, it is desirable to separate the rotational and vibrational temperatures from the translational temperature.

Recently, detailed computations of segmented-type arc heaters such as NASA's 20 MW Aerodynamic Heating Facility (AHF)

and 60 MW Interaction Heating Facility (IHF) have been performed using a modern numerical method. The simulation codes are respectively named ARCFLO2, ARCFLO3 and ARCFLO4 [8–12]. In those analysis models, an axisymmetric two-dimensional flow field was assumed which included the heating section with a turbulence model and a radiation model. A one-temperature or a two-temperature model was adopted for the thermophysical model. On the other hand, the authors [13–15] have performed numerical simulations for the flow field in a 20 kW constrictor-type arc-heated wind tunnel of Kyushu University (KU). This arc-heated wind tunnel has slight differences in the heating section compared to the segmented-type ones. In their previous works [13–15], it has been indicated that there appears an arc column, which has a very high-temperature and a fully-dissociated/ionized flow region in the constrictor section. In Ref [16], it has been reported that the heat transfer by the radiation plays an important role in this region.

For 20 kW KU that is relatively small size, turbulence behavior is not significant because of small Reynolds number. In such a small arc-heated wind tunnel, radiation becomes more important as well as molecular heat transfer. On the other hand, as a facility becomes larger, turbulent heat transfer becomes more important compared with molecular heat transfer. In such a large facility, turbulence and radiation play dominant role in heat-transfer process from the high-temperature core region to the cold gas region near the wall. Thus, it is very important to correctly model the effects of turbulence and radiation in the heating section, in addition to accurate reproduction of thermochemical nonequilibrium in the expansion section.

The present paper is concerned with the effects of heat transfers by radiation and turbulence in large-scale arc-heated flow simulation. In the present study, a sophisticated radiation-model equation was coupled with the flow-field and electric-field equations. In order to predict the effect of turbulence properly, we introduced a representative low-Reynolds-number two-equation turbulence model, which was proposed by Abe et al. [17] (AKN k-ε). Moreover, for detailed simulation of the expansion flow in the nozzle section, it was also needed to treat the rotational temperature separately from the translational temperature. Thus, the presented flow-field was described by the Navier-Stokes equations with a multi-temperature model, including translational (T_{tr}), rotational (T_{rot}), vibrational (T_{vib}) and electron (T_e) temperatures, to deal with the thermal nonequilibrium more properly.

2 Mathematical Formulation

Figure 1 shows a schematic view of a segmented-type arc heater such as 60 MW IHF. This arc heater is composed of constrictor, throat, nozzle section and two electrode chambers. The test gas such as argon, nitrogen and air is injected from holes on the constrictor wall. For 60 MW IHF, length and diameter of the constrictor section are about 3900 mm and 80 mm, respectively. The throat diameter is 60 mm. The nozzle geometry of 60 MW IHF is conical with half angle of 10 deg and the nozzle-exit diameter is 152 mm. An arc discharge is generated on the cathode and attaches to the anode surface. The test gas injected into the constrictor in subsonic condition is heated by the arc discharge and expands through the nozzle. Then the high-enthalpy flow is exhausted to the vacuum chamber in the tunnel system.

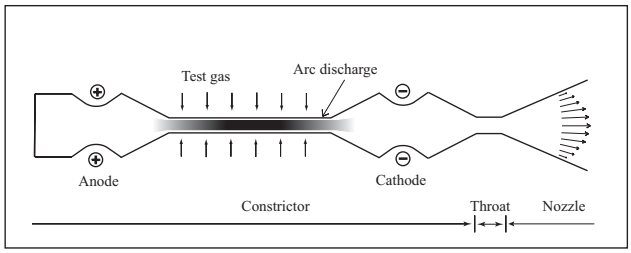

Fig. 1 Schematic view of a segmented-type arc heater

2.1 Governing Equations

In this study, the following assumptions were introduced. I) The flow is turbulent, steady, continuum and axisymmetric. II) Air is employed as test gas. III) The flow field is in thermochemical nonequilibrium and the temperature is separated into translational ($T_{\rm tr}$), rotational ($T_{\rm rot}$), vibrational ($T_{\rm vib}$) and electron ($T_{\rm e}$) temperatures. However, the electronic-excitation energy mode and the electron energy are assumed to equilibrate (the electronic-excitation temperature: $T_{\rm ex} = T_{\rm e}$). IV) Lorentz force, Hall current and ion slip can be neglected because the arc current is too small to induce an effective magnetic field. V) Radiation is considered.

The flow field was described by the Reynolds-Averaged Navier-Stokes (RANS) equations with a multi-temperature model and the equation of state. The RANS equations were composed of total mass, momentum, total energy, species mass, vibration energy, rotation energy and electron energy conservations. The equation system can be written in vector form as follows:

$$\frac{\partial \mathbf{Q}}{\partial t} + \frac{\partial \mathbf{F}}{\partial x_j} = \frac{\partial \mathbf{F}_{\rm v}}{\partial x_j} + \frac{\partial \mathbf{F}_{\rm rad}}{\partial x_j} + \mathbf{W}. \tag{1}$$

The conservative vector is expressed as $\mathbf{Q} = [\rho,\ \rho u_i,\ E,\ \rho_s,\ E_{\rm rot},\ E_{\rm vib},\ E_{\rm e}]$. Furthermore, $\mathbf{F}$, $\mathbf{F}_{\rm v}$ and $\mathbf{F}_{\rm rad}$ show the vectors of inviscid, viscous and radiation terms, respectively. Finally, $\mathbf{W}$ denotes the vector of source term. The equation of state can be expressed as

$$p = \sum_{s \neq {\rm e}} \rho_s R_s T_{\rm tr} + \rho_{\rm e} R_{\rm e} T_{\rm e} = \rho \hat{R} T_{\rm tr} + p_{\rm e}. \tag{2}$$

The electric-field equation was derived from the Maxwell equations and a generalized form of Ohm's law:

$$\nabla \cdot (\sigma \nabla \phi) = \nabla \cdot \left(\frac{\sigma}{e n_{\rm e}} \nabla p_{\rm e} \right), \tag{3}$$

where σ represents the electric conductivity and $n_{\rm e}$ is the number density of electrons. The current-density vector was calculated by the electric potential and the electron pressure:

$$\mathbf{j} = \sigma \left(-\nabla \phi + \frac{\sigma}{e n_{\rm e}} \nabla p_{\rm e} \right). \tag{4}$$

The Joule-heating rate $S_{\rm joule}$ can thus be given by

$$S_{\rm joule} = \frac{\mathbf{j}^2}{\sigma}. \tag{5}$$

2.2 Transport Properties

Transport properties, such as viscosity, thermal conductivity and binary diffusion coefficients for a mixture gas were evaluated by Yos' formula, which is based on the first Chapman-Enskog approximation. The collision cross sections were given by Gupta's works [18]. The diffusion coefficients were expressed by the formula of Curtiss and Hirschfelder [19]. Ambipolar diffusion was assumed for charged species as $D_s^a = (1 + T_{\rm e}/T_{\rm tr}) D_s$, where D_s is the effective diffusion coefficient of the ionic species.

2.3 Thermochemical Nonequilibrium

As for chemical reactions in high-temperature air, it was assumed that the test gas consisted of 11 chemical species (N_2, O_2, NO, N_2^+, O_2^+, NO^+, N, O, N^+, O^+ and e^-) and 49 reactions. The chemical reaction rate was determined with an Arrhenius type form. The reaction rate coefficients were obtained from Park's work [20]. Moreover, the backward reaction rate was evaluated from the corresponding equilibrium constant. The equilibrium constants, being functions of only temperature, were calculated by the curve-fit formula in Ref. [21].

We considered the energy transfer between each of the internal energy modes; translation-rotation (T-R) [22], translation-vibration (T-V) [23, 24], translation-electron (T-e) [25–27], rotation-vibration (R-V) [22], rotation-electron (R-e) [28, 29] and vibration-electron (V-e) [30].

2.4 Turbulence Model

In the present study, AKN k-ε model developed by Abe et al. [17] was introduced. We can write the turbulence transport equations regarding the turbulent kinetic energy (k) and its dissipation rate (ε) as

$$\frac{\partial \rho k}{\partial t} + \frac{\partial \rho k u_j}{\partial x_j} = \frac{\partial}{\partial x_j} \left\{ \left(\mu + \frac{\mu_{\rm t}}{\sigma_k} \right) \frac{\partial k}{\partial x_j} \right\} + P_k - \rho \varepsilon, \tag{6}$$

$$\frac{\partial \rho\varepsilon}{\partial t} + \frac{\partial}{\partial x_j}\left(\rho\varepsilon u_j\right) = \frac{\partial}{\partial x_j}\left\{\left(\mu + \frac{\mu_t}{\sigma_\varepsilon}\right)\frac{\partial \varepsilon}{\partial x_j}\right\} + C_{\varepsilon 1} f_{\varepsilon 1}\frac{\varepsilon}{k}P_k - C_{\varepsilon 2} f_{\varepsilon 2}\rho\frac{\varepsilon^2}{k}, \quad (7)$$

where P_k is the production term. The turbulent viscosity can be obtained from

$$\mu_t = C_\mu f_\mu \rho \frac{k^2}{\varepsilon}. \quad (8)$$

In Eqs (6) $\sim$ (8), C_μ, σ_k, σ_ε, $C_{\varepsilon 1}$ and $C_{\varepsilon 2}$ are the model constants and f_μ, $f_{\varepsilon 1}$ and $f_{\varepsilon 2}$ denote the model functions. The turbulent heat conductivity was evaluated using the turbulent Prandtl number Pr_t and the specific heat at constant pressure C_p by

$$\lambda_t = \frac{C_p \mu_t}{Pr_t}. \quad (9)$$

In the present study, Pr_t was set to 0.9.

2.5 Radiative Transport Equation

We introduced two assumptions into the present radiation calculation as follows; I) Effects of scattering were neglected. II) The radiation field was independent of time. Here, considering a ray emitting an infinitesimal element at a given position from a point in the one-dimensional coordinate, "s", the radiative transport equation can be expressed as

$$\cos\theta \frac{dI_\lambda}{ds} = \kappa_\lambda (B_\lambda - I_\lambda), \quad (10)$$

where I_λ, κ_λ and B_λ represent the radiation properties at a given wavelength, λ, referred to as intensity, absorption coefficient and blackbody function, respectively. Note that the absorption coefficient, κ_λ, includes the induced emission. Moreover, θ shows the angle between the ray and the s coordinate. The radiative heat flux at a given wavelength emitted to the infinitesimal element was evaluated over the entire solid angle,

$$q_\lambda^{\mathrm{rad}} = \int I_\lambda \cos\theta d\Omega. \quad (11)$$

Integrating Eq. (11) over all wavelengths, the total radiative heat flux can be obtained as

$$q^{\mathrm{rad}} = \int q_\lambda^{\mathrm{rad}} d\lambda. \quad (12)$$

3 Numerical Procedure

3.1 General

The governing equations were transformed to the generalized coordinate system and solved using a finite volume approach. All the flow properties were set at the center of a control volume. In the flow field equations, the inviscid fluxes were evaluated using the AUSMDV scheme [31] and all the viscous terms were calculated with the second-order central difference method. The spacial accuracy was thus basically kept to the second order.

The time integration was performed using an implicit time-marching method. The governing equation system was transferred into the delta form and the solution was updated at each time step. When we dealt with the thermochemical nonequilibrium flow, we needed to introduce a robust and effective time-integration scheme to overcome the stiffness caused by a large time-scale difference between the chemical reactions and the fluid motion that leaded to a severe restriction of the CFL condition. We employed the Lower-Upper Symmetric Gauss Seidel (LU-SGS) method [32] coupled with the point-implicit method [33].

The electric-field equations were discretized by the finite volume formulation and the numerical flux was evaluated by the second-order central difference method. The GMRES method [34] was used as the matrix solver for the electric-field equations and sufficient convergence was reached at each time step.

3.2 Boundary Conditions

At the inlet of 60 MW facility, the flow was injected in a subsonic condition, and the static pressure was extrapolated from the interior grid points. The other flow properties were calculated by the specified total temperature and the mass-flow rate. At the nozzle exit, the flow was supersonic for most part, except for the boundary layer near the nozzle wall. In the supersonic region, all the flow properties were determined from the zeroth extrapolation. At the electrode walls, non-

slip condition for velocity and non-catalytic condition for mass concentration were imposed. Furthermore, no pressure gradients normal to the wall were assumed. The wall temperature, T_w, was determined by a radiative equilibrium equation; $\varepsilon\sigma T_w^4 = q_w^{\text{conv}} + q_w^{\text{rad}}$, where $\varepsilon = 0.3$ and $\sigma = 5.67 \times 10^{-8}$ W/K^{4}m^2 are the emissivity and the Stefan-Boltzmann constant, respectively. Here, q_w represents the heat flux injected into the anode wall. Along the symmetric axis, an axisymmetric condition was imposed.

No currents were allowed to pass though the inlet and the nozzle exit. An equipotential condition was set at the electrode wall, where $V = 0$ at the cathode surface and $V = V_0$ at the anode surface. By using the input current I, the total current I^n in the flow field, and the arc voltage V^n at the nth step, the arc voltage V^{n+1} at $(n+1)$th time step can be given as

$$V^{n+1} = V^n + \Delta V^n, \quad \Delta V^n = \omega \left(\frac{I}{I^n} - 1 \right) V^n, \tag{13}$$

where ω represents a relaxation coefficient.

3.3 Calculation conditions

In the present calculation, the input parameters of 60 MW IHF are the arc current (I) and the mass-flow rate ($\dot{m}$). The computational condition of $I = 6000$ A and $\dot{m} = 380$ g/sec is defined as 'the baseline case.' The computational domain and grids for 60 MW IHF are shown in Fig. 2.

4 Results and Discussion

Figure 3 illustrates the translational temperature and axial velocity contours for the baseline case. In the present model, the one-temperature model was utilized in the heating section (the electrode chambers and constrictor), whereas the four-temperature model was adopted in the nozzle section. This assumption was originally introduced in order to decrease a numerical stiffness. However, since there expected to be frequent collisions between species and the flow field is close to thermally equilibrium in the heating section,

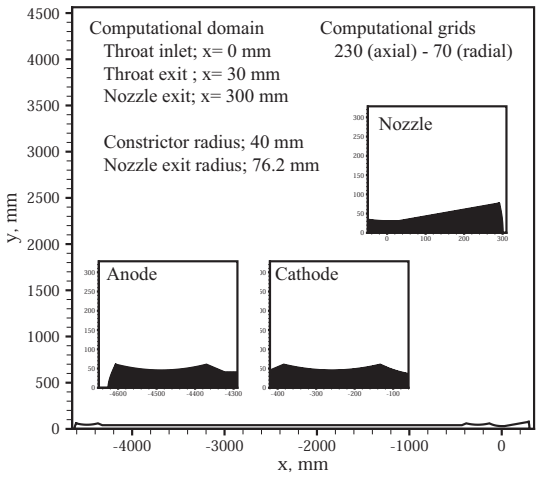

Fig. 2 Computational domain and grids for 60 MW IHF

it is thought that the assumption has less influence on the present flow-field prediction. A high-temperature region is formed around the center axis in the constrictor and the translational temperature reaches a maximum value of 11320 K. A cold gas region appears near the wall and temperature gradient in the radial direction becomes large. It seems that the plasma flow is rapidly cooled with expansion passing through the throat and nozzle sections. The flow injected from the constrictor wall is accelerated to $u \sim 500$ m/sec through the constrictor and the cathode chamber. The Mach number is still lower than unity and the plasma flow is subsonic in the heating section, although the Mach number distribution is not shown here. It is seen that the arc-heated flow is rapidly accelerated, which leads to choke at the throat exit. Then, the axial velocity approaches to a maximum value of 5240 m/sec on the center axis at the nozzle exit.

The distributions of the mole fractions along the center axis for the baseline case are illustrated in Fig. 4. Throughout the flow field, atomic nitrogen and oxygen are dominant chemical species caused by the dissociation reactions. Moreover, it seems that small amount of the electrons and the ion species such as ionized-atomic nitrogen

and oxygen are also contained in the arc column in the heating section. The electrons are primary careers of the electric current in the arc column from the anode to the cathode. In the nozzle section, the recombination reaction of atomic nitrogen occurs very slowly and the expansion flow results in being totally frozen.

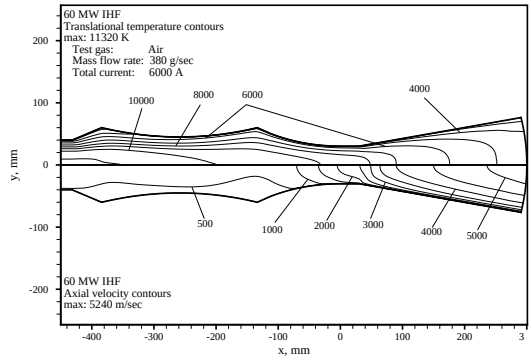

Fig. 3 Contours of translational temperature (above) and axial velocity (below) in 60 MW IHF for the baseline case

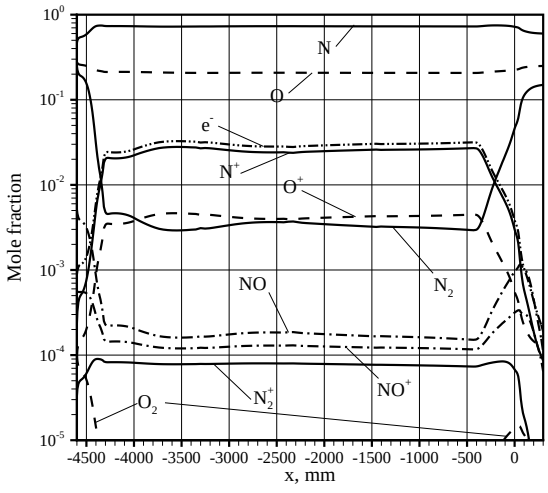

Fig. 4 Axial profile of mole fractions along the center axis in 60 MW IHF for the baseline case

We investigate effects of turbulence in the facilities, in addition to the radiation heat transfer. Firstly, the viscosity-ratio contours for the baseline case are illustrated in Fig. 5. In the present study, the viscosity ratio is defined as the ratio of the turbulence viscosity divided by the molecular viscosity (μ_t/μ). It is indicated that the viscosity ratio is large in the cathode chamber in spite of the lower velocity. Reynolds number of the plasma flow in 60 MW IHF is generally larger than that of the other arc-heating facilities, because the scale is larger and the flow maintains higher density in the heating section due to large amount of mass-flow rate. This fact is the reason why turbulence is strong, though the flow-velocity magnitude is relatively lower. The large viscosity ratio distributes near the wall in the cathode chamber and the throat section, which reaches a maximum value of 278 near the throat inlet. It is clarified that the effects of turbulence in 60 MW IHF are more a great deal dominant.

Next, we compare the predicted heat transfers by radiation and turbulence and discuss their contributions to the flow fields. Figures 6 and 7 depict radial profiles of the heat fluxes and the translational temperature for the baseline case at the constrictor exit ($x = -450$ mm) and the throat inlet ($x = 0$ mm), respectively. It is indicated that both turbulence and radiation are significant mechanisms of heat transfer from the core flow to the cold gas at the constrictor exit. On the other hand, the radiation transport far becomes low at the throat inlet, while the heat transfer is almost borne by the turbulence.

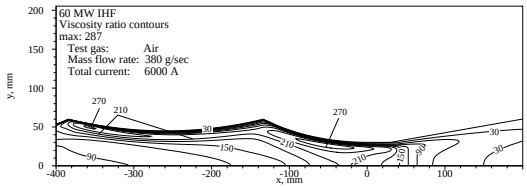

Fig. 5 Viscosity ratio contours in 60 MW IHF for the baseline case

We compare the computational results with the corresponding experimental data [35], i.e., the arc voltage, the mass-averaged enthalpy at the nozzle exit, the chamber pressure at the con-

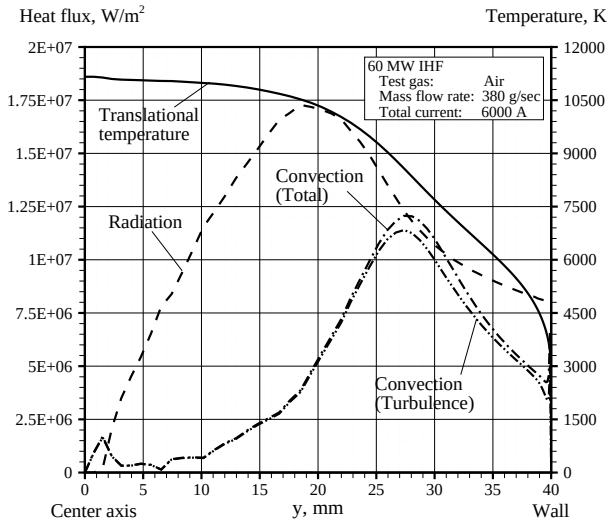

Fig. 6 Radial profiles of heat fluxes and temperature at the constrictor exit ($x = -450$ mm) for the baseline case of 60 MW IHF

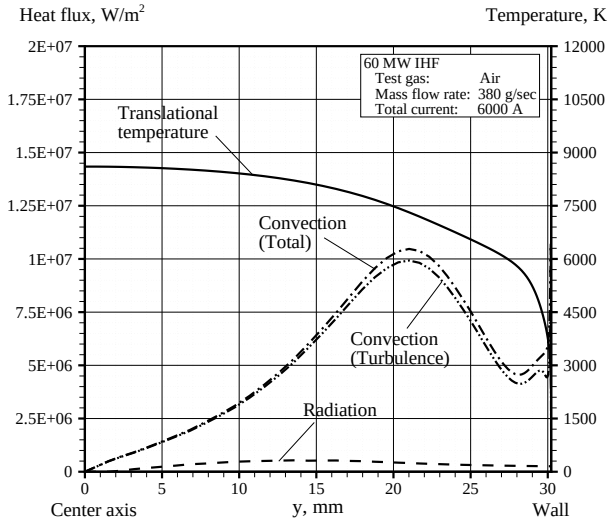

Fig. 7 Radial profiles of heat fluxes and temperature at the throat inlet ($x = 0$ mm) for the baseline case of 60 MW IHF

strictor exit and the heat efficiency. The mass-averaged enthalpy at the nozzle exit was evaluated by using the energy-balance method. In the present study, the mass-averaged enthalpy h_{av} is determined using the following expression:

$$h_{\mathrm{av}} = \int_0^{\mathrm{R}} \rho u h r dr \Big/ \int_0^{\mathrm{R}} \rho u r dr. \qquad (14)$$

In addition, the predicted heat-efficiency η is defined with the heat fluxes, the arc voltage and the current as follows: $\eta = 1 - \left(q^{\mathrm{conv}} + q^{\mathrm{rad}}\right)/IV$, where q^{conv} and q^{rad} represent the convective and radiative heat fluxes on the wall, respectively.

Figures 8, 9, 10 and 11 show the comparisons of the arc voltage, the mass-averaged enthalpy, the chamber pressure and the heat efficiency, respectively. The data are plotted against the mass-flow rate for two electric current conditions ($I = 3000$ and 6000 A). The predicted voltage tends to increase with the mass-flow rate and is maintained virtually constant for two electric current conditions. There exist underestimations of about $500 - 1000$ V in the arc voltage prediction. On the other hand, the other properties predicted, i.e., the mass-averaged enthalpy, the chamber pressure and the heat efficiency, agree well those of the experimental data not only qualitatively but also quantitatively under various operating conditions.

In general, radiation transport plays an important role in arc-heated flow simulation. Additionally, as a facility scale becomes large, the flow field in the facility is highly affected by turbulence transport. Hence, it is significant to introduce a proper turbulence model as well as a radiation model in order to accurately predict arc-heated flow properties.

5 Conclusions

Numerical simulations of plasma flows in the NASA 60 MW IHF were successfully performed for various input-current and mass-flow rate conditions, coupled with the electric-field and radiative-field calculations tightly. The flow field in the arc-heating facilities were assumed to be in thermochemical nonequilibrium. To express thermal nonequilibrium properly, a four-temperature model was introduced into the present analysis model, which separates temperature into translational, rotational, vibrational

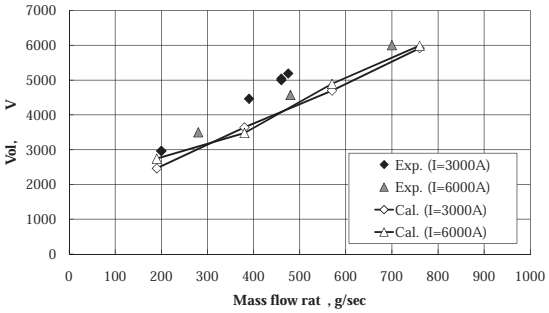

Fig. 8 Comparison of arc voltage for 60 MW IHF

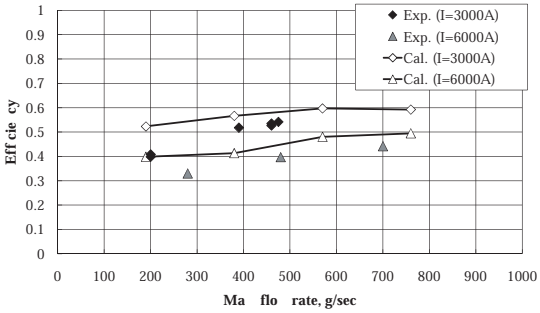

Fig. 11 Comparison of heat efficiency for 60 MW IHF

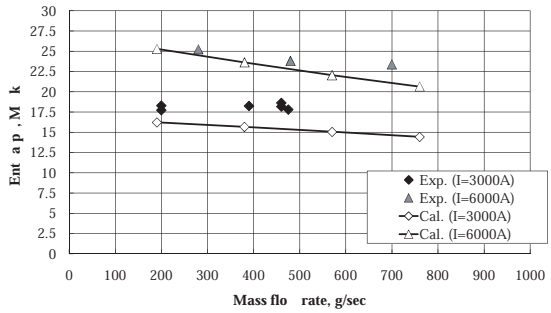

Fig. 9 Comparison of mass-averaged enthalpy at the nozzle exit for 60 MW IHF

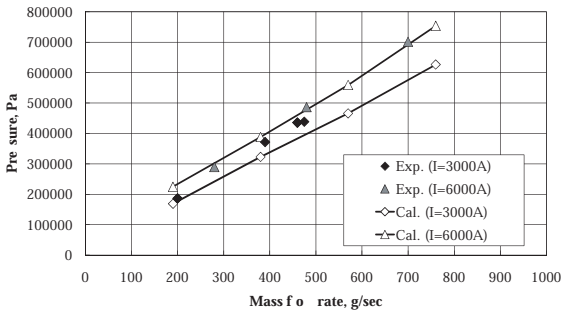

Fig. 10 Comparison of chamber pressure at the constrictor exit for 60 MW IHF

and electron ones, and detailed internal energy-exchange models were utilized. In addition, the effects of radiation and turbulence transports in the arc-heated flow fields were investigated with the three-band radiation model and AKN model which is one of the low-Reynolds number $k-\varepsilon$ models.

Fundamental features of high-enthalpy flows in the large-scale facilities, e.g., the arc column and the supersonic expansion, could be reproduced and detailed distributions of the flow-field properties were obtained. In the nozzle section, it was elucidated that less recombination reactions occur in the nozzle sections of the 60 MW facility and the expansion flow is close to be chemically frozen. Heat transfers by radiation and turbulence in the large-scale facilities were investigated in detail and those transport phenomena were quantitatively clarified. Radiation in the constrictor section where there exists high-temperature gas plays a key role to carry energy from the arc column to the cold gas and the walls. Furthermore, it is elucidated that the turbulence also gave influence on the momentum and heat transfer processes in the heating section of the large-scale arc-heated wind tunnel.

In order to validate the present numerical model, the computed data were compared with those of the corresponding experiments, i.e., the arc voltage, the mass-averaged enthalpy, the chamber pressure and the heat efficiency. Quantitative agreements with the experimental data were shown for the various calculation conditions. However, the predicted arc voltage tended to be less in several hundreds compared with the measured ones.

Acknowledgments

The computation was mainly carried out using the computer facilities at Research Institute for Information Technology, Kyushu University. The first author is supported by Research Fellowships of the Japan Society for the Promotion of Science for Young Scientists.

5.1 Copyright Statement

References

[1] M. A. Birkan. "Arcjets and Arc Heaters: An Overview of Research Status and Needs". *Journal of Propulsion and Power*, Vol. 12, No. 6, pp. 1011–1017, Nov.-Dec. 1996.

[2] D. S. Babikian, N. K. J. M. Gopaul, and C. Park. "Measurement and Analysis of Nitric Oxide Radiation in an Arcjet Flow". *Journal of Thermophysics and Heat Transfer*, Vol. 8, No. 4, pp. 737–743, Oct.-Dec. 1994.

[3] C. Park and S.-H. Lee. "Validation of Multitemperature Nozzle Flow Code". *Journal of Thermophysics and Heat Transfer*, Vol. 9, No. 1, pp. 9–16, Jan.-Mar. 1995.

[4] T. Gökçen, C. S. Park, M. E. Newfield, and D. G. Fletcher. "Computational Simulation of Emission Spectra from Shock-Layer Flows in an Arcjet Facility". *Journal of Thermophysics and Heat Transfer*, Vol. 12, No. 2, pp. 180–189, April-June 1998.

[5] G. Colonna and M. Capitelli. "Self-Consistent Model of Chemical, Vibrational, Electron Kinetics in Nozzle Expansion". *Journal of Thermophysics and Heat Transfer*, Vol. 15, No. 3, pp. 308–316, July-Sept. 2001.

[6] K. Abe, T. Kameyama, H. Kihara, M. Nishida, K. Ito, and H. Tanno. "Computation and Experiment of Nonequilibrium Nozzle Flow of Arc-heated Air". *Journal of Thermophysics and Heat Transfer*, Vol. 19, No. 4, pp. 428–434, 2005.

[7] G. Colonna and M. Capitelli. "Boltzmann and Master Equations for Magnetohydrodynamics in Weakly Ionized Gases". *Journal of Thermophysics and Heat Transfer*, Vol. 22, No. 3, pp. 414–423, July-Sept. 2008.

[8] K. H. Kim, O. H. Rho, and C. Park. "Navier-Stokes Computation of Flows in Arc Heaters". *Journal of Thermophysics and Heat Transfer*, Vol. 14, No. 2, pp. 250–258, April-June 2000.

[9] T. Sakai, K. Sawada, and M. Mitsuda. "Application of Planck-Rosseland-Gray Model for High-Enthalpy Arc Heaters". *Journal of Thermophysics and Heat Transfer*, Vol. 15, No. 2, pp. 176–183, April-June 2001.

[10] T. Sakai and J. Olejniczak. "Improvements in a Navier-Stokes Code for Arc Heater Flows". *AIAA Paper 2003-3782*, 2003.

[11] J.-P. Lee, C. Kim, and K.-H. Kim. "Accurate Computations of Arc-Heater Flows Using Two-Equation Turbulence Models". *Journal of Thermophysics and Heat Transfer*, Vol. 21, No. 1, pp. 67–76, Jan.-Mar. 2007.

[12] T. Sakai. "Computational Simulation of High-Enthalpy Arc Heater Flows". *Journal of Thermophysics and Heat Transfer*, Vol. 21, No. 1, pp. 77–85, Jan.-Mar. 2007.

[13] Y. Takahashi, H. Kihara, and K. Abe. "Numerical Simulation of Plasma Flows in a 20kW Arc-Heated Wind Tunnel Using Multi-Temperature Model". In *APCOM' 07-EPMESC XI*, GS16-4, Kyoto, Japan, Dec. 3-6 2007.

[14] Y. Takahashi, H. Kihara, and K. Abe. "Numerical Investigation of Thermochemical Nonequilibrium Flow Field in a 20kW Arc Heater Coupled with Electric Field Calculation". In *Rarefied Gas Dynamics, 26th International Symposium on Rarefied Gas Dynamics*, pp. 883–888, Kyoto, Japan, July 20-26 2008.

[15] Y. Takahashi, H. Kihara, and K. Abe. "Numerical Investigation of Nonequilibrium Plasma

Flows in Constrictor- and Segmented-Type Arc Heaters". *Journal of Thermophysics and Heat Transfer*, Vol. 24, No. 1, pp. 31–39, 2010.

[16] Y. Takahashi, H. Kihara, and K. Abe. "The Effects of Radiative Heat Transfer in Arc-Heated Nonequilibrium Flow Simulation". *Journal of Physics D: Applied Physics*, Vol. 43, No. 18, p. 185201, 2010.

[17] K. Abe, T. Kondoh, and Y. Nagano. "A New Turbulence Model for Predicting Fluid Flow and Heat Transfer in Separating and Reattaching Flows - I. Flow Field Calculations". *International Journal of Heat and Mass Transfer*, Vol. 37, No. 1, pp. 139–151, 1994.

[18] R. N. Gupta, J. M. Yos, R. A. Thompson, and K.-P. Lee. "A Review of Reaction Rates and Thermodynamic and Transport Properties for an 11-Species Air Model for Chemical and Thermal Nonequilibrium Calculations to 30000 K". *NASA RP-1232*, Aug. 1990.

[19] C. F. Curtiss and J. O. Hirschfelder. "Transport Properties of Multicomponent Gas Mixture". *Journal of Chemical Physics*, Vol. 17, No. 6, pp. 550–555, June 1949.

[20] C. Park. "Assessment of a Two-Temperature Kinetic Model for Dissociating and Weakly Ionizing Nitrogen". *Journal of Thermophysics and Heat Transfer*, Vol. 2, No. 1, pp. 8–16, Jan.-March 1988.

[21] C. Park. *Nonequilibrium Hypersonic Aerothermodynamics*. Wiley, New York, 1990.

[22] C. Park. "Rotational Relaxation of N_2 Behind a Strong Shock Wave". *Journal of Thermophysics and Heat Transfer*, Vol. 18, No. 4, pp. 527–533, Oct.-Dec. 2004.

[23] R. C. Millikan and D. R. White. "Systematics of Vibrational Relaxation". *The Journal of Chemical Physics*, Vol. 39, No. 12, pp. 3209–3213, Dec. 1963.

[24] C. Park. "Problems of Rate Chemistry in the Flight Regimes of Aeroassisted Orbital Transfer Vehicles". *AIAA Paper 84-1730*, 1984.

[25] J. P. Appleton and K. N. C. Bray. "The Conservation Equations for a Nonequilibrium Plasma". *Journal of Fluid Mechanics*, Vol. 20, No. 4, pp. 659–672, June 1964.

[26] M. Mitchner and C. H. K. Jr. *Partially Ionized Gases*. Wiley, New York, 1973.

[27] J.-H. Lee and D. R. White. "Thermal Design of Aeroassisted Orbital Transfer Vehicles". In H. F. Nelson, editor, *Basic Governing Equations for the Flight Regimes of Aeroassisted Orbital Transfer Vehicles (Progress in Astronautics and Aeronautics)*, Vol. 96, pp. 3–53. AIAA, New York, 1985.

[28] M. Nishida and M. Matsumoto. "Thermochemical Nonequilibrium in Rapidly Expanding Flows of High-Temperature Air". *Zeitschrift für Naturforcuhung, Teil A: Physik, Physikalische Chemie, Kosmophysik*, Vol. 52, pp. 358–368, 1997.

[29] S. S. Lazdinis and S. L. Petrie. "Free Electron and Vibrational Temperature Nonequilibrium in High Temperature Nitrogen". *Physics of Fluids*, Vol. 17, No. 8, pp. 1539–1546, Aug. 1974.

[30] J.-H. Lee. "Electron-Impact Vibrational Relaxation in High-Temperature Nitrogen". *Journal of Thermophysics and Heat Transfer*, Vol. 7, No. 3, pp. 399–405, July-Sept. 1993.

[31] Y. Wada and M.-S. Liou. "A Flux Splitting Scheme with High-Resolution and Robustness for Discontinuities". *AIAA Paper 94-0083*, 1994.

[32] A. Jameson and S. Yoon. "Lower-Upper Implicit Schemes with Multiple Grids for the Euler Equations". *AIAA Journal*, Vol. 25, No. 7, pp. 929–935, July 1987.

[33] T. R. A. Bussing and E. M. Murman. "Finite-Volume Method for the Calculation of Compressible Chemically Reacting Flows". *AIAA Journal*, Vol. 26, No. 9, pp. 1070–1078, 1988.

[34] Y. Saad and M. H. Schultz. "GMRES: A Generalized Minimal Residual Algorithm for Solving Nonsymmetric Linear Systems". *SIAM Journal on Scientific and Statistical Computing*, Vol. 7, No. 3, pp. 856–869, July 1986.

[35] T. M. Hightower, J. A. Balboni, C. L. M. Donald, K. F. Anderson, and E. R. Martinez. "Enthalpy by Energy Balance for Aerodynamic Heating Facility at NASA Ames Research Center Arc Jet Complex". In *Proceedings of the 48th International Instrumentation Symposium*, Vol. 420, Instrumentation, Systems, and Automation Society, San Diego, CA, 2002.